Int. J. Electrochem. Sci., 15 **(2020)** 4869 – 4883, doi: 10.20964/2020.06.28

International Journal of
ELECTROCHEMICAL
SCIENCE
www.electrochemsci.org

Metal Sulfide Nanoparticles Anchored N, S Co-doped Porous Carbon Nanofibers as Highly Efficient Bifunctional Electrocatalysts for Oxygen Reduction/Evolution Reactions

Qijian Niu[*,1,2,3], *Oluwafunmilola Ola*[3], *Binling Chen*[3], *Yanqiu Zhu*[3], *Yongde Xia*[3], *Guiping Ma*[*,2]

[1] School of Agricultural Equipment Engineering, Jiangsu University, Zhenjiang, Jiangsu, 212013, China
[2] Key Laboratory of carbon fiber and functional polymers, Ministry of Education, Beijing University of Chemical Technology, Beijing, 100029, P. R. China
[3] College of Engineering, Mathematics and Physical Sciences, University of Exeter, Exeter, EX4 4QF, UK
[*]E-mail: niuqijian1989@163.com

Received: 5 February 2020 / *Accepted:* 29 March 2020 / *Published:* 10 May 2020

Developing multi-functional electrocatalysts is a key for new energy techniques, such as fuel cells, metal-air batteries, and water splitting. In this paper, a bifunctional (ORR/OER) electrocatalysts, metal sulfide nanoparticles anchored N, S co-doped porous carbon nanofibers were successfully synthesized by a simultaneous carbonization and sulfurization of ZIFs/PAN electrospun composite nanofibers. The as-prepared material Zn/Co-ZIFs/PAN-CS-800 catalyst exhibited an excellent electrocatalytic performance in both ORR and OER. Such excellent ORR and OER performance comes from the active metal sulfide species, N, S co-doping effect, porous structure, and good conductivity. Our method can be used to produce other metal sulfide nanoparticles combined with N, S co-doped porous carbon materials with potential applications in the field of energy storage and conversion.

Keywords: electrospinning, porous carbon nanofiber, metal sulfide, N, S co-doped, ORR/OER

1. INTRODUCTION

Oxygen reduction/evolution reactions (ORR/OER) are the key reactions of new energy techniques (fuel cells, metal-air batteries, and water splitting). Currently, the best ORR electrocatalysts are still Pt-based materials, whereas IrO_2 and RuO_2 are the best ones for OER. However, their poor stability, high price and limited resources on earth limit their application in large scale. Thus, it is very important to develop high activity and stability, low price and earth-abundant electrocatalysts for ORR and OER [1-3].

Up to now, transition metal-based ORR/OER electrocatalysts including transition metal carbides[4, 5], nitrides[6, 7], oxides[8, 9], phosphide[10, 11], sulfides[12, 13], and nanocarbon materials[14, 15] have been studied. It was reported that the composite of transition metal sulfide and carbon material can improve its conductivity, corrosion resistance and catalytic activity[16]. Liu et al. prepared an effective ORR/OER electrocatalyst Co/Co_xS_y@S,N-co-doped porous carbon fiber, which was derived from S,N containing MOFs[17]. Ma et al. produced a Co_9S_8-modified N, S, and P ternary-doped 3D graphene electrode catalyst as a promising bifunctional catalyst for both the ORR and OER under corrosive conditions[18]. Liu et al. made a highly dispersed CoS_x nanocrystals coupled with N-doped porous carbon (CoS_x@NMC) bifunctional catalyst using Fe/Co dual tuning N,S-containing polymer as the carbon precursor[19]. Chen et al. developed a bi-metallic sulfide/carbon nanocomposite as a multifunctional electrocatalyst via a one-step simultaneous carbonization and sulfurization method [12, 20].

Electrospinning is an easy, fast and efficient method for the preparation of nanofibers[21, 22] Recent studies have shown that carbon-based nanofiber catalysts prepared from the precursor electrospun nanofiber have shown excellent properties[23, 24]. However, metal sulfide nanoparticles embedded in N, S-codoped porous carbon nanofibers derived from ZIFs/PAN nanofibers is rarely reported.

In the work, we designed a composite electrospun nanofiber where metal sulfide nanoparticles embedded in N, S co-doped porous carbon nanofibers. This preparation method can be achieved via a facile carbonization and sulfurization procedure by using Zn/Co-ZIFs/PAN nanofiber as a precursor. Among the prepared samples, the optimal one Zn/Co-ZIFs/PAN-CS-800 exhibited an excellent ORR and OER performance with an outstanding stability in alkaline media. This work opens a new path for the design of highly active metal sulfide nanoparticles anchored N, S co-doped porous carbon nanofiber electrocatalysts.

2. EXPERIMENTAL SECTION

2.1 Materials

Polyacrylonitrile (PAN, M_w = 150000 g mol^{-1}), zinc nitrate hexahydrate ($Zn(NO_3)_2{\cdot}6H_2O$), cobalt nitrate hexahydrate ($Co(NO_3)_2{\cdot}6H_2O$), 2-Methylimidazole ($C_4H_6N_2$, MIM), methanol (MeOH), ethanol (EtOH, ≥99.7%), potassium hydroxide (KOH, 98%), and N,N-dimethylformamide (DMF) were all purchased from Aladdin Chemical Reagent Co. Nafion solution (5 wt%), common commercial 20 wt% Pt/C catalyst, and commercial RuO_2 (99.9%) catalyst was all purchased from Sigma-Aldrich. All obtained chemicals were used as purchased without any further purification except any noted by special notification[25].

2.2 Preparation of ZIFs-8, ZIFs-67, bimetal Zn/Co-ZIFs nanocrystals

ZIFs-8, ZIFs-67, bimetal Zn/Co-ZIFs nanocrystals were synthesized by a modified method[26]. 1.5 mmol metallic nitrates ($Zn(NO_3)_2{\cdot}6H_2O$, $Co(NO_3)_2{\cdot}6H_2O$, and the mixture of 0.5 mmol

$Zn(NO_3)_2 \cdot 6H_2O$ and 1.0 mmol $Co(NO_3)_2 \cdot 6H_2O$) was uniformly dispersed in 15.0 mL methanol solution, and 6.0 mmol 2-methylimidazole was dissolved into 5.0 mL methanol solution under stirring for 30 min at room temperature, respectively. Subsequently, the 5 mL methanol solution containing 6.0 mmol 2-methylimidazole was added to the above metallic nitrates solution. With continuous stirring for 12 h, the obtained ZIFs nanocrystals was collected by centrifugation, washed with methanol three times, and then dried at 60 ℃ for 12 h.

2.3 Preparation of ZIFs-8/PAN, ZIFs-67/PAN, and Zn/Co-ZIFs/PAN nanofibers

The 0.5 g PAN powder was dissolved into 4.5 g DMF solvent under stirring at 40℃ for 6 h. Subsequently, 1.0 g ZIFs nanocrystals powder was added into the above solution. With continuous stirring for 6 h, the obtained ZIFs/PAN/DMF solution was transferred into a 5.0 mL plastic syringe. Traditional electrospinning process was carried out with a high voltage of 20 kV and an extrusion rate of 0.6 mL h^{-1}. The obtained nanofibers were collected on the aluminum foil (~15 cm×~15 cm). The collect distance between the nozzle and the aluminum foil was 15 cm. The obtained ZIFs/PAN composite nanofiber film was easily peeled off from the collector and put into a vacuum oven overnight at a temperature of 80℃ to remove the residual solvents[27].

2.4 Preparation of metal sulfide nanoparticles anchoring on N, S co-doped porous carbon nanofibers electrocatalysts

Firstly, a typical pre-oxidation process was conducted at 280℃ for 2 h at a heating rate of 2 ℃ min^{-1} under air atmosphere. Secondly, the furnace was then heated to the target temperature (typically 600, 800, and 1000℃) with a heating rate of 5 ℃ min^{-1} under pure argon atmosphere; when the furnace temperature reached the target temperatures, the gas of hydrogen sulfide was introduced into the quartz tube with a flow rate of 50 mL min^{-1} and maintained at the target temperature for 1 h. The gas flow was then switched to argon alone with a flow rate of 60 mL min^{-1} while the furnace started to cool down to room temperature. The final product was collected from the quartz tube and labelled as ZIFs/PAN-CS-T, where CS stands for the carbonization and sulfurization process and T stands for target carbonization temperature.

2.5 Materials characterization

The morphologies and structures of the as-prepared samples were characterized by scanning electron microscopy (SEM; JSM-6701F, operating at 5 kV) and transmission electron microscopy (TEM; Tecnai G2 20 S-T win, operating at 200 kV). X-ray diffraction powder (XRD) patterns were recorded with Cu Kα radiation. N_2 gas sorptions were carried out on a Quantachrome Autosorb-iQ gas sorptometer via the conventional volumetric technique. Before gas analysis, the sample was evacuated for 3 hours at 200 ℃ under vacuum. X-ray photoelectron spectroscopy (XPS) were taken on an ESCLAB 250 spectrometer.

2.6 Electrochemical measurements

A conventional three-electrode system was employed to evaluate the electrocatalytic performance of the obtained catalysts on a CHI 660C electrochemical workstation. The catalyst modified GCE was the working electrode, a Ag/AgCl electrode (3.0 M KCl) was the reference electrode, and Pt wire was the counter electrode. The rotating ring disk electrode measurements for ORR were carried out on RRDE-3A (ALS Co., Ltd, Japan) in a N_2- or O_2- saturated 0.1 M KOH electrolyte solution at a scan rate of 10 mV s^{-1} at various rotation rates of 400, 625, 900, 1225, 1600, 2025, and 2500 rpm. For OER measurements, linear sweep voltammetry (LSV) were all recorded in a O_2-saturated 1.0 M KOH with scan rate of 10 mV s^{-1}. All the potentials were converted to the potential versus the reversible hydrogen electrode (RHE) according to E (RHE) = E (Ag/AgCl) + 0.21 V + 0.0591pH. All OER data are presented with 95% iR auto-compensation. In addition, the electron transfer number (n) was calculated from the Koutecky-Levich (K-L) equation:

$$\frac{1}{j} = \frac{1}{j_L} + \frac{1}{j_K} = \frac{1}{B\omega^{1/2}} + \frac{1}{j_K}$$

$$j_k = nFkC_0$$

$$B = 0.2nFC_0(D_0)^{2/3}V^{-1/6}$$

Where ω is the angular velocity, J is the measured current density, J_K and J_L are the kinetic and diffusion-limiting current densities. F is Faraday constant (96485 C mol^{-1}), D_0 is the diffusion coefficient of O_2 (1.9×10^{-5} cm^2 s^{-1}), v is the kinetic viscosity of the electrolyte (0.01 cm^2 s^{-1}) and C_0 is the bulk concentration of O_2 (1.2×10^{-6} mol cm^{-3}), n is the electron transfer number. B can be determined from the slope of the K-L plots, and then the electron transfer number n can be obtained[28,29].

3. RESULTS AND DISCUSSION

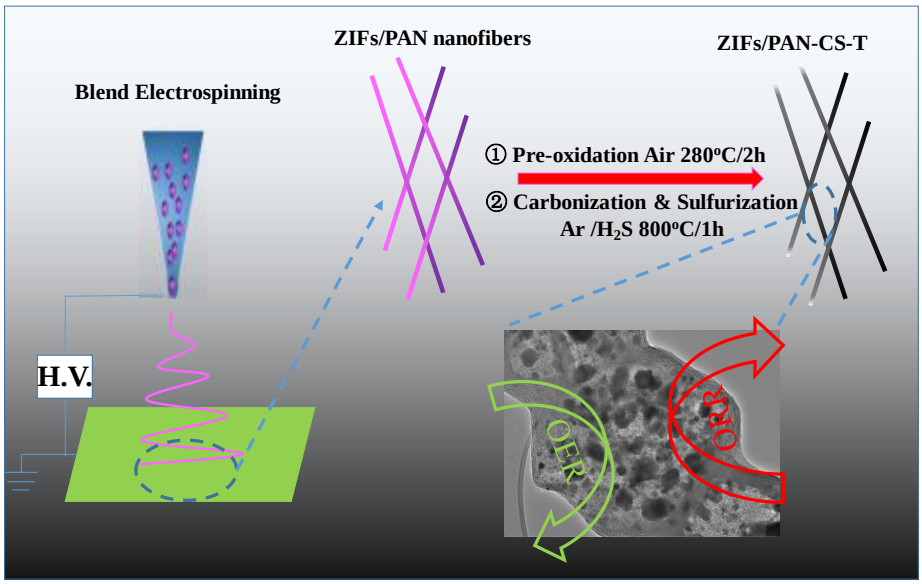

Scheme 1. Schematic illustration for the formation process of ZIFs/PAN-CS-T catalysts.

Scheme. 1 illustrates the preparation strategy of ZIFs/PAN-CS-T (see the Experimental Section for details). This process consists of two main steps: first, ZIFs/PAN nanofibers were prepared by a simple blend electrospinning method; second, a controlled simultaneous carbonization and sulfurization process was conducted to produce the ZIFs/PAN-CS-T.

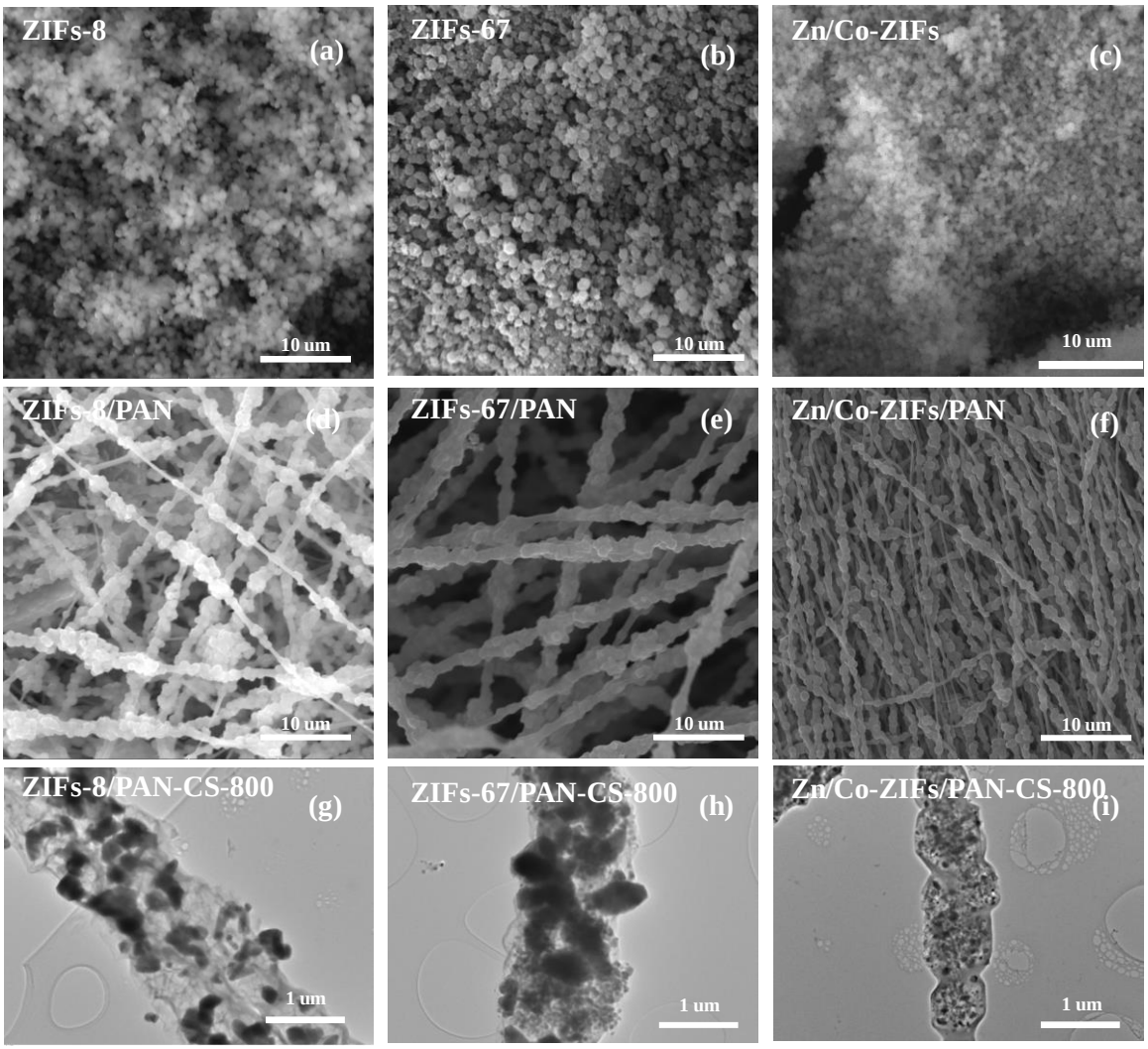

Figure 1. SEM images of (a) ZIFs-8; (b) ZIFs-67; (c) Zn/Co-ZIFs nanoparticles; (d) ZIFs-8/PAN; (e) ZIFs-67/PAN; (f) Zn/Co-ZIFs/PAN nanofibers; TEM images of (g) ZIFs-8/PAN-CS-800; (h) ZIFs-67/PAN-CS-800; (i) Zn/Co-ZIFs/PAN-CS-800 carbon nanofibers.

Fig. 1(a), (b) and (c) show the SEM images of origin ZIFs-8, ZIFs-67 and Zn/Co-ZIFs nanoparticles, respectively. It can be seen that the Zn/Co-ZIFs has a smaller particle size than that of origin ZIFs-8 and ZIFs-67. After electrospinning, ZIFs nanoparticles loaded in PAN polymer nanofiber to become ZIFs/PAN nanofibers with rough surfaces (Fig. 1(d), (e), (f)). After the carbonization and surfulzation process, obvious change of structure can be observed from the TEM images of Fig. 1(g), (h) and (i). Fig. 1(g) shows that nanoparticles were formed on the surface of ZIFs-8/PAN-CS-800, and some pore structure can be observed in the carbon nanofibers. Fig. 1(h) shows a severe agglomeration of nanoparticles in ZIFs-67/PAN-CS-800. In Fig. 1(i), uniform nanoparticles and pore structure can be

identified in Zn/Co-ZIFs/PAN-CS-800. The above images suggested that the Zn element in Zn/Co-ZIFs can not only adjust the size of ZIFs nanocrystals, but also reduce the agglomeration of metal nanoparticles in the smaple of Zn/Co-ZIFs/PAN-CS-800, which is helpful to the improvement of electrochemical properties.

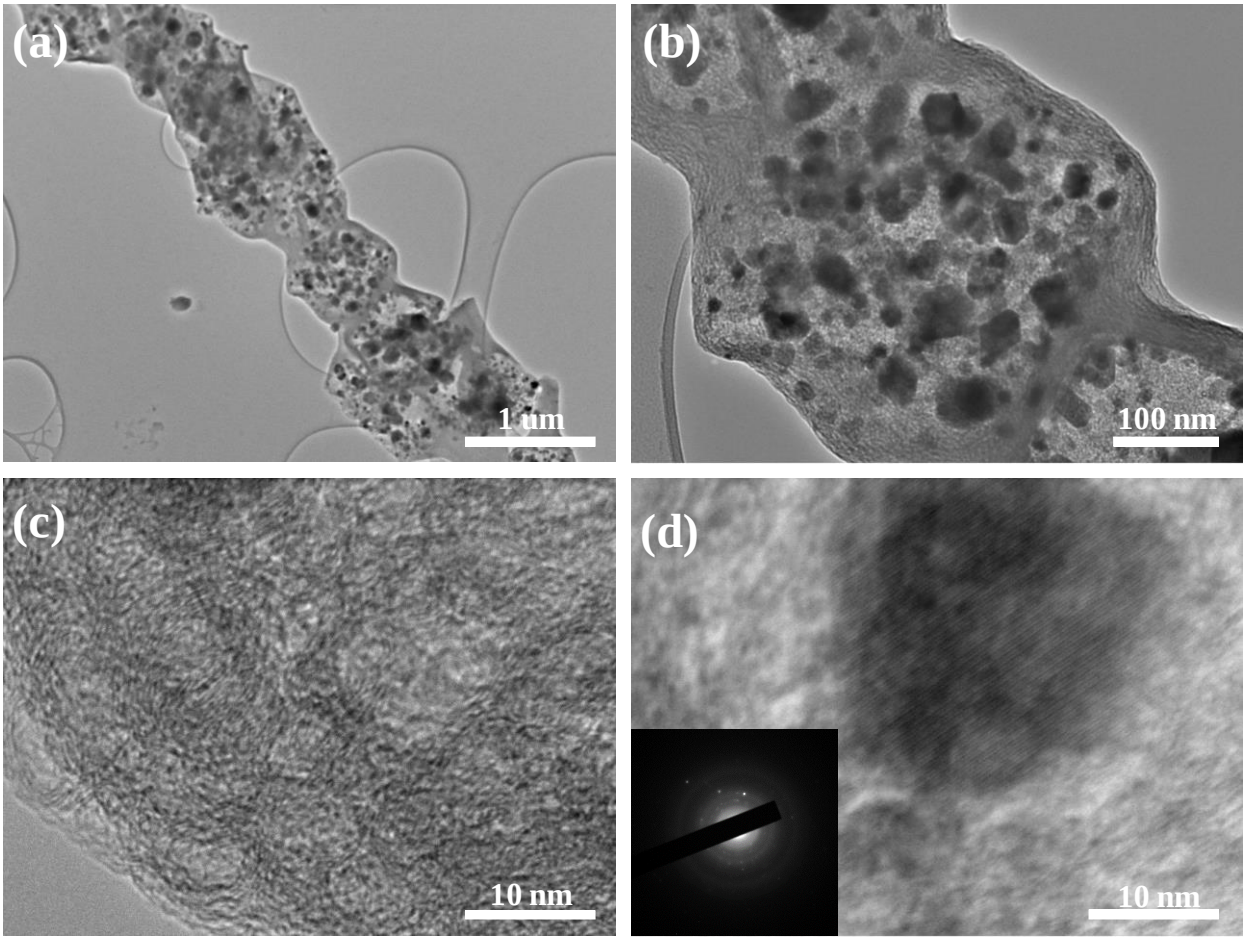

Figure 2. HR-TEM images of Zn/Co-ZIFs/PAN-CS-800 (Inset in Fig. 2(d) shows SAED pattern).

The microstructure and the crystalline phase of the Zn/Co-ZIFs/PAN-CS-800 nanofibers were investigated by HR-TEM and selected area electron diffraction (SAED). As shown in Fig. 2(a) and Fig. 2(b), TEM images obviously confirmed the presence of nanoparticles, and these nanoparticles were embedded in the pore of Zn/Co-ZIFs/PAN-CS-800 nanofibers in a good dispersion. Fig. 2(c) shows the HR-TEM image of graphitized carbon layer. It can been seen that the degree of graphitization is not very high, which may be caused by the N, S dopping effect. In addition, some pores can be seen in the carbon layer, which is caused by the metal evaporation. N, S dopping effect and pore structure are both beneficial to the improvement of electrochemical performance. Fig. 2(d) shows the HR-TEM image of a single nanoparticle; the inset image in Fig. 2(d) is the corresponding SAED pattern of the nanoparticle. The concentric circles pattern revealed the polycrystalline feature of the as-prepared metal sulfide nanoparticles.

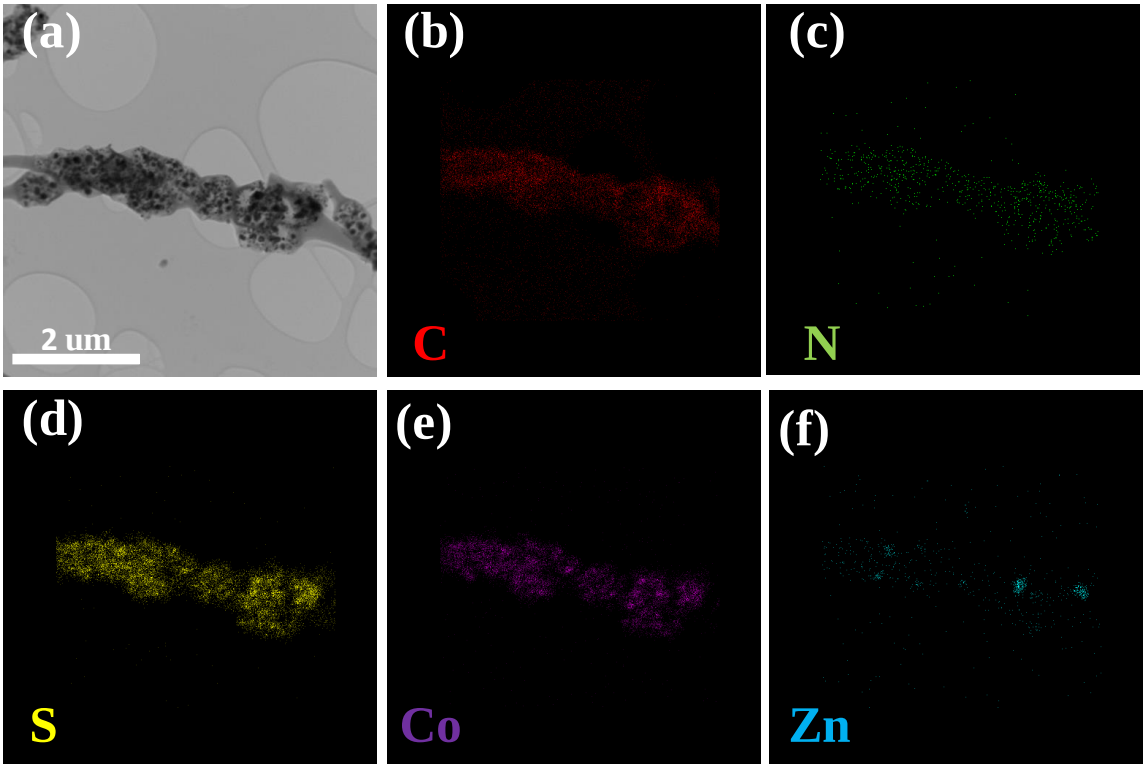

Figure 3. (a) TEM image and STEM mapping of the (b) C, (c) N, (d) S, (e) Co, (f) Zn elements for Zn/Co-ZIFs/PAN-CS-800 nanofibers.

The mapping images of the various elemental were obtained from the TEM image area (Fig. 3(a)) of Zn/Co-ZIFs/PAN-CS-800 nanofibers. It confirms the presence of element C, N, S, Co and Zn (Fig. 3(b),(c),(d),(e),(f)). Furthermore, Co element mainly existed in the form of nanoparticles, and S element not only existed in the nanoparticles, but also well distributed through the whole carbon nanofibers. Combined with the uniform distribution of N element in the carbon nanofibers, it can be confirmed the presence of N,S co-dopant as well as the formation of CoS nanoparticles in the carbon nanofibers. The Zn element mainly concentrates on the nanoparticles outside the carbon nanofibers. These mapping results are in consistent to the observations in Fig. 1(g).

Fig. 4 shows the XRD patterns of the prepared samples. ZIFs-8/PAN-CS-800 only has some diffraction peaks, which suggests the formation of ZnS in composite nanofibers. Relative diffraction peaks of CoS crystalline phase can be distinguished in ZIFs-67/PAN-CS-800. Notably, the characteristic diffraction peaks of Zn/Co-ZIFs/PAN-CS-800 shows the presence of ZnS and CoS crystalline phase. CoS phase became stronger and ZnS phase disappeared with the increase of the calcination temperature from 600 to 1000 ^{o}C, which was attributed the evaporation of Zn at higher temperatures. In details, the boiling point of the metallic zinc is 906 ^{o}C, when the carbonization temperature reaches 1000 ^{o}C, the metallic Zn is able to completely evaporate. When the temperature is below 900 ^{o}C, the residual Zn element forms as ZnS crystals.

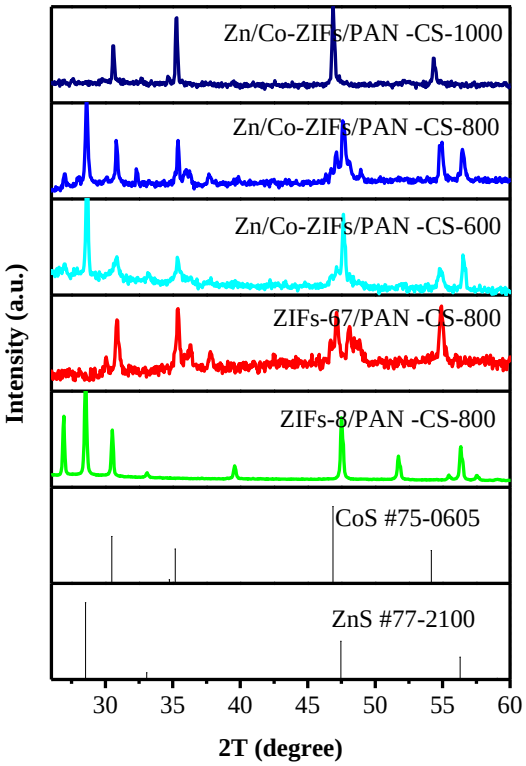

Figure 4. XRD patterns of different samples and referenced ones.

The XPS measurement is used to characterize the chemical composition. The full XPS spectra (Fig. 5(a)) of Zn/Co-ZIFs/PAN-CS-800 reveal the presence of C (72.29 at. %), O (11.09 at. %), N (6.25 at. %), S (8.39 at. %), Zn (0.66 at. %), and Co (1.33 at. %) element. The high-resolution C 1s spectrum (Fig. 5(b)) can be decomposed into three individual peaks, the peak at 284.8 eV corresponds to the standard peak of C=C. Besides, the peak at 285.5 eV confirms the existence of saturated carbon species of C−S, C−O, C−N, whereas the peak at 288.1 eV corresponds to the unsaturated carbon species of C=O, C=N. Fig. 5(c) shows the N 1s spectrum of Zn/Co-ZIFs/PAN-CS-800 nanofibers.

It can be split into four peaks at around 398.5, 399.6, 401.5, and 403.2 eV, corresponding to pyridinic N, pyrrolic N, graphitic N, and oxidized N, respectively[30, 31]. It has been reported that these N species played an important role in the ORR/OER process, where pyridinic N can improve the onset potential, while graphitic N determines the limiting current of ORR. As can be seen from the S 2p XPS spectrum, the split S species at around 163.9 and 165.5 eV corresponds to S $2p_{3/2}$ and $2p_{1/2}$ in CoS, respectively, and the peak at 162.1 and 169.0 eV corresponds to thiophene S and SO_x, respectively[13, 32]. Based on the XPS results, the N doping level in Zn/Co-ZIFs/PAN-CS-800 nanofibers is about 6.25 at%; however, it is difficult to evaluate the doping level of S separately in the whole materials.

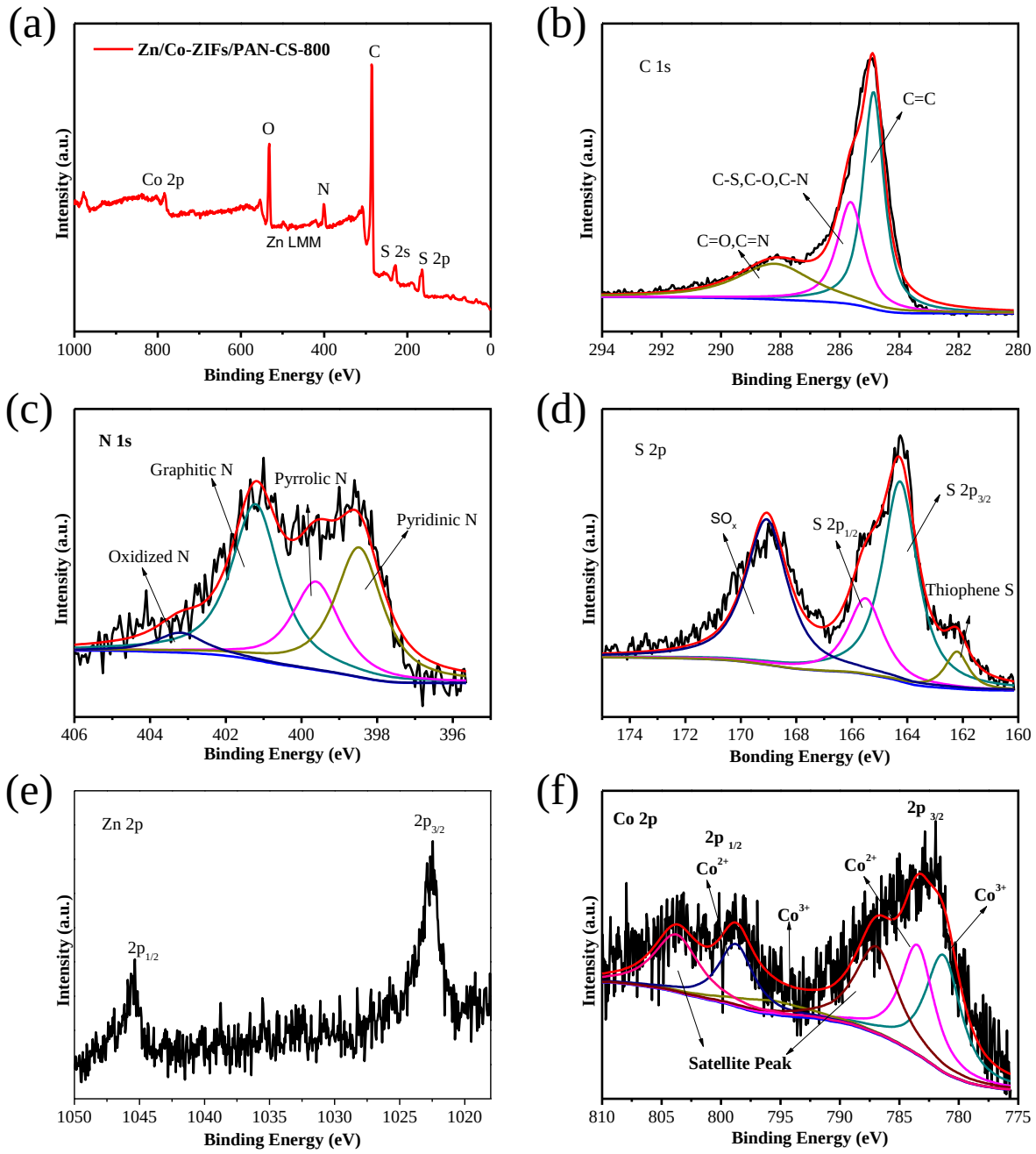

Figure 5. (a) XPS and the HR-XPS spectra of (b) C 1s, (c) N 1s, (d) S 2p, (e) Zn 2p and (f) Co 2p of Zn/Co-ZIFs/PAN-CS-800 nanofibers.

The peaks at 1046.2 and 1022.8 eV corresponds to Zn $2p_{3/2}$ and Zn $2p_{1/2}$, respectively (Fig. 5(e))[33]. Moreover, the decomposition of the Co 2p spectrum is shown in Fig. 5(f). The characteristic peaks at 781.6 and 783.3 eV can be attributed to $Co^{3+}2p_{3/2}$ and Co^{2+} $2p_{3/2}$, respectively. The other spin-orbit component appearing at 795.6 and 798.7 eV is for $Co^{3+}2p_{1/2}$ and $Co^{2+}2p_{1/2}$, respectively[34].

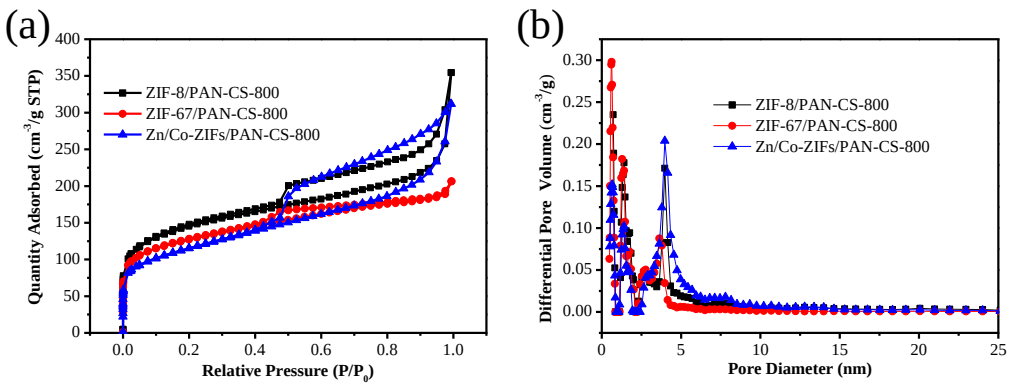

Figure 6. (a) The N_2 adsorption-desorption isotherm of different samples and (b) their pore distribution curves.

The N_2 adsorption-desorption experiments of the prepared samples were conducted to test the surface areas and pore size distributions. As shown in Fig. 6(a), the calculated Brunauer-Emmett-Teller (BET) surface area of ZIFs-8/PAN-CS-800, ZIFs-67/PAN-CS-800, and Zn/Co-ZIFs/PAN-CS-800 is 513.9, 446.3, and 407.6 m^2 g^{-1}, respectively. The higher surface area of ZIFs-8/PAN-CS-800 is due to the formation of porous carbon. Fig. 6(b) shows the pore size distribution curves of ZIFs-8/PAN-CS-800, ZIFs-67/PAN-CS-800, and Zn/Co-ZIFs/PAN-CS-800. ZIFs-8/PAN-CS-800 and ZIFs-67/PAN-CS-800 exhibit a dominant microporous structure, while Zn/Co-ZIFs/PAN-CS-800 displays a primary mesoporous structure with a pore size centered at 4 nm. The presence of mesoporous structure in Zn/Co-ZIFs/PAN-CS-800 is not only favorable to improve its surface area for more catalytic active sites exposure, but also to enhance the mass transport of electrocatalysis.

For ORR measurements, the LSV curves (Fig. 7(a)) obtained at 1600 rpm show that Zn/Co-ZIFs/PAN-CS-800 exhibits an onset potential of 0.90 V and a half-wave potential of 0.83 V, which are better than other samples. The onset potential and half-wave potential of Zn/Co-ZIFs/PAN-CS-800 are slightly negative shifted compared to those of 20 wt% Pt/C. The effect of carbonization temperature experiments (Fig. 7(b)) show that Zn/Co-ZIFs/PAN-CS-800 has the highest ORR performance among all the catalysts produced at various temperatures. It is believed that CoS nanoparticles and N, S dopants combined with porous carbon structure are beneficial to the ORR activity. Fig. 4(c) shows the LSV curves of Zn/Co-ZIFs/PAN-CS-800 under various rotation speeds. The K-L curves (Fig. 4(d)) exhibit linear relationships at 0.41-0.71 V, very close to that of 20 wt% Pt/C catalyst, which suggests a four-electron ORR process, further indicates the high ORR activity of Zn/Co-ZIFs/PAN-CS-800. Remarkably, the Zn/Co-ZIFs/PAN-CS-800 catalyst exhibited almost no current density fluctuation with the addition of 2 mL methanol; however, a sharp decrease of current density can be observed in 20 wt % Pt/C under the same conditions (Fig. 5(e)), confirming the high methanol tolerance of our prepared catalysts. The long-term stability of the Zn/Co-ZIFs/PAN-CS-800 catalyst was tested, where chronoamperometric i−t response over a period of 36 000 s on a RDE at 1600 rpm and 10 mV s^{-1} in O_2-saturated 0.1 M KOH was performed.

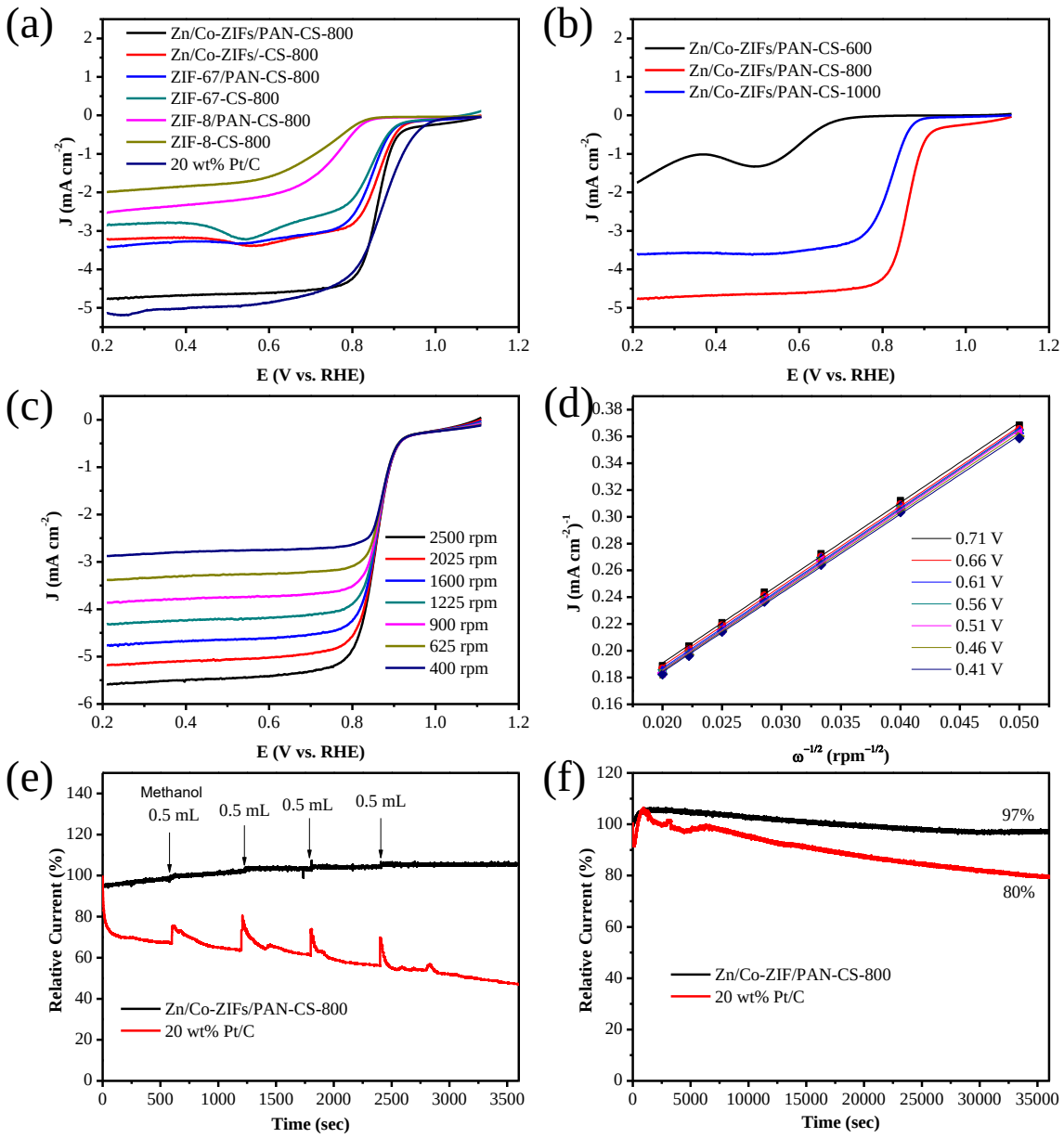

Figure 7. (a) LSV curves of different samples; (b) LSV curves of Zn/Co-ZIFs/PAN-CS in different temperatures; (c) LSV curves of Zn/Co-ZIFs/PAN-CS-800 at different rotation speeds; (d) Koutecky-Levich (K-L) curves; (e) Methanol tolerance of Zn/Co-ZIFs/PAN-CS-800 and 20 wt% Pt/C; (f) Electrocatalytic stabilities of Zn/Co-ZIFs/PAN-CS-800 and 20 wt% Pt/C in O_2-saturated 0.1 m KOH solution at 0.71 V (vs. RHE).

As shown in Fig. 7(f), after 36 000 s of the following operation, ~97% of the initial current can be remained for the Zn/Co-ZIFs/PAN-CS-800 catalyst, whereas only ~80% for 20 wt% Pt/C was remained, indicating the higher durability of the Zn/Co-ZIFs/PAN-CS-800 catalyst.

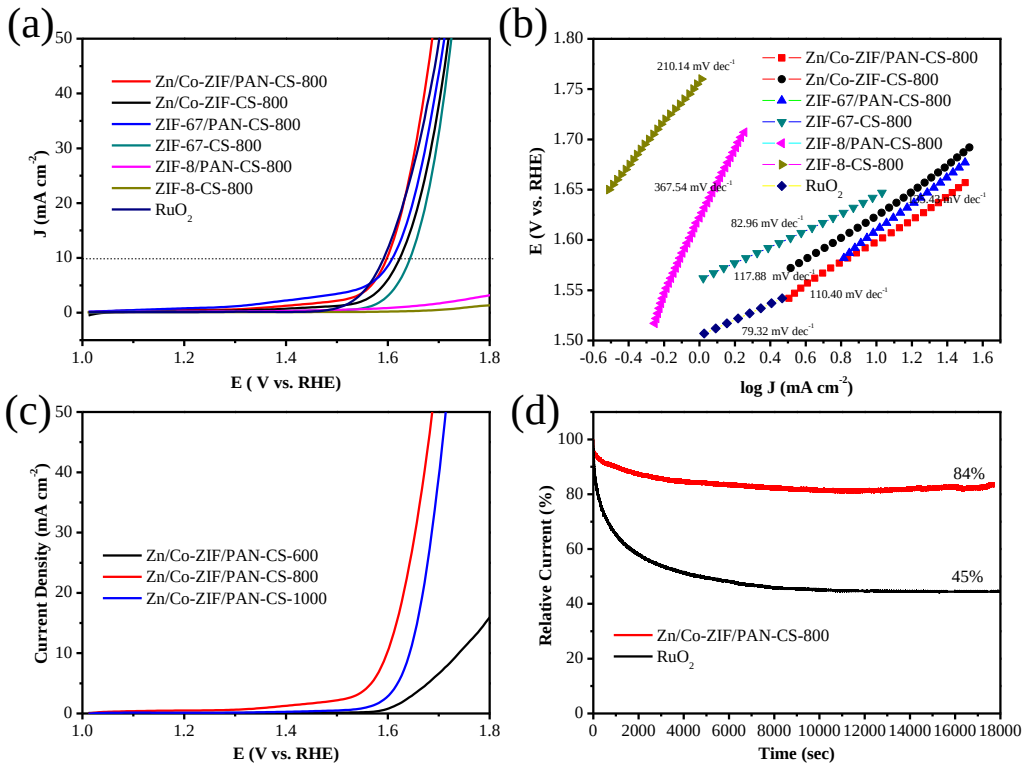

Figure 8. (a) LSV curves of different samples and RuO_2 with a 95% iR compensation; (b) Tafel slopes of different samples; (c) LSV curves of Zn/Co-ZIFs/PAN-CS in different temperatures; (d) Electrocatalytic stabilities of Zn/Co-ZIFs/PAN-CS-800 and RuO_2 in O_2-saturated 1.0 M KOH aqueous solution at 1.60 V (vs. RHE).

The OER activities of different samples were tested in O_2-saturated 1.0 M KOH under 1600 rpm. As shown in Fig. 8(a), the potential at 10 mA cm^{-2} of Zn/Co-ZIFs/PAN-CS-800 nanofibers (367 mV) is very close to that of RuO_2 catalyst, indicating its high activity toward OER. In addition, the pyrolysis temperature of 800 °C was found to be the optimal temperature for achieving a highly active OER performance (Fig. 8(c)). As shown in Fig. 8(b), it can be found that the Tafel slopes of ZIFs-8-CS-800, ZIFs-8/PAN-CS-800, ZIFs-67-CS-800, ZIFs-67/PAN-CS-800, Zn/Co-ZIFs-CS-800, Zn/Co-ZIFs/PAN-CS-800 and RuO_2 is 210.14, 367.54, 82.96, 135.43, 117.88, 110.40 and 79.32 mV dec^{-1} respectively. Apparently, ZIFs-67-CS-800 has a similar value of Tafel slope to RuO_2 catalyst, but it is not the optimal catalyst. Zn/Co-ZIFs/PAN-CS-800 exhibits the superior OER performance than other catalysts; this is consistent with the diverse ORR performances, confirming its bifunctional performances. Additionally, the chronoamperometric i-t response measurements were assessed at a constant potential at 1.60 V for 18000 s to determine the durability of OER. As can be seen in Fig. 8(d), Zn/Co-ZIFs/PAN-CS-800 apparently presented only a slight current attenuation of 84% after 18000 s, while the RuO_2 electrode showed 45% over the same period of time, suggesting that Zn/Co-ZIFs/PAN-CS-800 has an improved long-term stability. Comparisons with other catalysts are listed in the Table 1

Table 1. Comparison with other catalysts

Catalysts	E_{onset} for ORR	E_{10mA} for OER	Reference
$Fe_1Co_1S_x$@NSPC	0.98 V	390 mV	[13]
Co/Co_xS_y@SNCS-800	0.85 V	307 mV	[17]
CoS_x@NMC	0.90 V	570 mV	[19]
Co_9S_8/NSCNFs-850	-	302 mV	[32]
Co_9S_8/N,S-CNS	0.90 V	350 mV	[35]
$CoO@Co_3O_4$/NSG-650	0.79 V	460 mV	[36]
Co_9S_8/CNT	0.94 V	369 mV	[37]
Co_9S_8@CT-800	-	390 mV	[38]
NSC-1000	0.913 V	-	[39]
Zn/Co-ZIFs/PAN-CS-800	0.90 V	367 mV	This work

4. CONCLUSION

In summary, we have developed a simple method for the production of metal sulfide nanoparticles anchored N, S co-doped porous carbon nanofiber electrocatalysts with an excellent bifunctional ORR/OER performance by a carbonization and sulfurization of ZIFs/PAN electrospun nanofibers. The presence of CoS and N, S co-doped porous structure were confirmed to be the two important factors for the high ORR/OER performance. CoS nanoparticles in the carbon layer not only enhanced electron transfer of O_2 catalysis between CoS and the carbon layer, but also enhanced the stability of the catalyst. The electrocatalysis results proved that Zn/Co-ZIFs/PAN-CS-800 possessed an excellent catalytic activity for ORR and OER, which are comparable to those of 20 wt% Pt/C and RuO_2, respectively.

References

1. K. Shen, X.D. Chen, J.Y. Chen and W.Y. Li, *ACS Catal.*, 6 (2016) 5887.
2. Z.F. Huang, J. Wang, Y.C. Peng, C.Y. Jung, A. Fisher and X. Wang, *Adv. Energy Mater*., 7 (2017) 1700544.
3. Y.H. Qian, I.A. Khan and D. Zhao, *Small*, 13 (2017) 1701143.

4. L. Song, T. Wang, Y.L Wang, H.R. Xue, X.L Fan, H. Guo, W. Xia, H. Gong and J.P. He, *ACS Appl. Mater. Interfaces*, 9 (2017) 3713.
5. G.Y. Ren, X.Y. Lu, Y.N Li, Y. Zhu, L.M. Dai and L. Jiang, *ACS Appl. Mater. Interfaces*, 8 (2016) 4118.
6. S.L. Zhao, M. Li, M. Han, D.D. Xu, J. Yang, Y. Lin, N.E. Shi, Y.N. Lu, R. Yang, B.T. Liu, Z.H. Dai and J.C. Bao, *Adv. Funct. Mater*., 28 (2018) 1706018.
7. X.X. Huang, Z.Y. Yang, B. Dong, Y.Z. Wang, T.Y. Tang and Y.L. Hou, *Nanoscale*, 9 (2017) 8102.
8. D. Dong, Y. Liu and J.H. Li, *Part. Part. Syst. Char*., 33 (2016) 887.
9. A. Aijaz, J. Masa, C. Rosler, W. Xia, P. Weide, A.J. Botz, R.A. Fischer, W. Schuhmann and M. Muhler, *Angew. Chem. Int. Ed*., 55 (2016) 4087.
10. Y.F. Cheng, F. Liao, W. Shen, L.B. Liu, B.B. Jiang, Y.Q. Li and M.W. Shao, *Nanoscale*, 9 (2017) 18977.
11. S. Shanmugam, A. Sivanantham, M. Matsunaga, U. Simon and T. Osaka, *Electrochim. Acta*, 297 (2019) 749.
12. B.L. Chen, G.P. Ma, Y.Q. Zhu, J.B. Wang, W. Xiong and Y.D. Xia, *J. Power Sources*, 334 (2016) 112.
13. W.G. Fang, P. Dai, H.B. Hu, T.T. Jiang, H.Z. Dong and M.Z. Wu, *Appl. Surf. Sci*., 505 (2020) 144212.
14. B.L. Chen, G.P. Ma, Y.Q. Zhu and Y.D. Xia, *Sci. Rep.*, 7 (2017) 5266.
15. C.G Hu and L.M. Dai, *Angew. Chem. Int. Ed*., 55 (2016) 11736.
16. X.Y. Yu and X.W. Lou, *Adv. Energy Mater*., 8 (2018) 1701592.
17. S.W. Liu, X. Zhang, G.Z. Wang, Y.X. Zhang and H.M. Zhang, *ACS Appl. Mater. Interfaces*, 9 (2017) 34269.
18. X.X. Ma, X.H. Dai and X.Q. He, *ACS Sustainable Chem. Eng*., 5 (2017) 9848.
19. C. Liu, F. Dong, M.J. Wu, Y.X.Wang, N.N. Xu, X. Wang, J.L. Qiao, P.H. Shi and H.T. Huang, *J. Power Sources*, 438 (2019) 226953.
20. B.L. Chen, R. Li, G.P. Ma, X.L. Gou, Y.Q. Zhu and Y.D. Xia, *Nanoscale*, 7 (2015) 20674.
21. W.M. Li, M.X. Li, C. Wang, Y. Wei and X.F. Lu, *Appl. Surf. Sci*., 506 (2020) 144680.
22. Y. Si, J.Y. Yu, X.M. Tang, J.L. Ge and B. Ding, *Nat. Commun*., 5 (2014) 5802.
23. Q.J. Niu, J.X. Guo, B.L. Chen, J. Nie, X.D. Guo, G.P. Ma, *Carbon*, 114 (2017) 250.
24. J.X. Guo, Q.J. Niu, Y.C. Yuan, I. Maitlo, J. Nie and G.P. Ma, *Appl. Surf. Sci*., 416 (2017) 118.
25. S.W Liu, X. Zhang, G.Z. Wang, Y.X. Zhang and H.M. Zhang, *ACS Appl. Mater. Interfaces*, 9 (2017) 34269.
26. R.B. Wu, X.K. Qian, K. Zhou, J. Wei, J. Lou and P.M. Ajayan, *ACS Nano*, 8 (2014) 6297.
27. Q.J. Niu, B.L. Chen, J.X. Guo, J. Nie, X.D. Guo and G.P. Ma, *Nano Micro Lett*., 11 (2019).
28. B. You, N. Jiang, M.L. Sheng, W.S. Drisdell, J.k. Yano and Y.J. Sun, *ACS Catal*., 5 (2015) 7068.
29. C. Wu, Y.H. Zhang, D. Dong, H.M. Xie and J.H. Li, *Nanoscale*, 5 (2015) 7068.
30. R. Sibul, E.K. Põldsepp, U. Mäeorg, M. Merisalu, A. Kikas, V. Kisand, A. Treshchalov, V. Sammelselg and K. Tammeveski, *Electrochem. Commun*., 109 (2019) 106603.
31. Z.W. Hu, Z.Y. Guo, Z.P. Zhang, M.L. Dou and F. Wang, *ACS Appl. Mater. Interfaces*, 10 (2018) 12651.
32. L.L. Wu, Q.S. Wang, J. Li, Y. Long, Y. Liu, S.Y. Song and H.J. Zhang, *Small*, 14 (2018) e1704035.
33. Z. Yu, Y. Bai, S.M. Zhang, Y.X. Liu, N.Q. Zhang and K.N. Sun, *J. Mater. Chem*. A, 6 (2018) 10441.
34. J.T. Ren and Z.Y. Yuan, *ACS Sustainable Chem. Eng*., 7 (2019) 10121
35. C. Wu, Y.H. Zhang, D. Dong, H.M. Xie, and J.H. Li, *Nanoscale*, 9 (2017) 12432.
36. X.B. Huang, J.Q. Wang, H.L. Bao, X.K. Zhang, and Y.M. Huang, *ACS Appl. Mater. Interfaces*, 10 (2018) 7180.

37. H. Li, Z. Guo, and X.W. Wang, *J. Mater. Chem*. A, 5 (2017) 21353.
38. T. Liu, L.M. Zhang, and Y. Tian, *J. Mater. Chem*. A, 6 (2018) 5935.
39. Y.Q. Li, H.B. Xu, H.Y. Huang, L.G. Gao, Y.Y. Zhao, and T.L. Ma, *Electrochimica Acta*, 254 (2017) 148.